Suspended Core Fibers for the Transmission of Cylindrical Vector Modes

Hong Ji, *Member, OSA*, Yinlan Ruan, *Member, OSA*, Shahraam Afshar Vahid, *Member, OSA*, Heike Ebendorff-Heidepriem, *Member, OSA*, and Tanya M. Monro, *Member, OSA*

***Abstract*— This paper presents a study of propagation of radially and azimuthally polarized cylindrical vector modes in six-strut suspended core fibers based on finite element simulations. The study shows large effective index differences in order of 10^{-3}-10^{-2} of these modes can be achieved in the suspended core fibers with core diameter of less than 2 μm, material index 1.45 of silica to 2.0 of tellurite and wavelength of 750 nm, allowing the stable propagation of the first higher order modes in doughnut shape within these fibers. The effective index difference and the field intensity of these cylindrical vector modes can be tuned by selecting appropriate fiber material and core size. The study shows that the suspended core fiber can be a competitive candidate for fiber-based high-resolution stimulated emission depletion (STED) nanoscopy application.**

***Index Terms*—Fiber optics, fibers polarization maintaining, fiber fluorescence microscopy, laser beam shaping, optical vortices, optical fiber device, polarization-selective devices.**

I. INTRODUCTION

CYLINDRICAL vector (CV) beams, including radially, azimuthally and hybrid polarized first higher order modes generated in an optical fiber, have cylindrical symmetry of field amplitude and non-uniform distribution of field polarization vectors. Based on these special properties, CV beams have found a wide range of applications as optical vortices including far-field nano/microscopy [1-5], particle acceleration [6], optical tweezers and trapping [7], materials processing and high efficiency laser machining [8, 9], classical optical and quantum communications [10-12]. CV beams with orbital angular momentum (OAM) comprise an orthogonal basis set of modes and have found applications for high bit-rate fiber communications [13, 14].

CV beams with doughnut shaped intensity pattern are essential for stimulated emission depletion (STED) nanoscopy in biomedical imaging and sensing applications [2-5], and it is this emerging application area that we focus on for the development of the new class of optical fibers described in this paper. In STED nanoscopy, a high intensity doughnut shaped beam with a dark central spot is used to bleach the fluorescence emission within the doughnut pattern, which allows only the fluorescence within the central dark spot to be detected and this enables subwavelength-scale resolution, beyond the diffraction limit. However, current STED nanoscopy systems are based on free space optics, which leads to complicated instrumentation as it requires two beams – the excitation and depletion beams – which must be aligned to each other, making the configuration susceptible to mechanical instability. As an alternative to this approach, the doughnut shaped first higher order modes in optical fibers have been explored for use in nanoscopy [15-17] to allow alignment and propagation of the two beams (a Gaussian beam and a doughnut beam, which are essentially required to realise a stimulated emission depletion), along a single fiber simultaneously. The resolution of a STED nanoscopy can be estimated with the equation (1) [18]:

$$\rho \approx \lambda\left(1+I_m/I_S\right)^{-0.5}/\left(2NA\right), \quad (1)$$

where ρ is the resolution in STED nanoscopy, λ is the depletion beam wavelength, I_m is the STED intensity at the doughnut crest (field intensity maximum along the doughnut rim) and I_S is the dye saturation intensity. To achieve nanoscale resolution, it is critical that the transverse doughnut shaped beam field distribution exhibits a large intensity contrast between the doughnut crest and the central dark spot [5].

Conventional optical fibers can in principle guide

The manuscript received at … for review. This work has been supported by ARC Georgina Sweet Laureate Fellowship grant to Tanya Monro.

H. Ji is with the Institute for Photonics and Advanced Sensing and the ARC Center for Nanoscale BioPhotonics, The University of Adelaide, Adelaide, SA, 5005, Australia (e-mail: Hong.Ji@ adelaide.edu.au).

Y.L. Ruan is with the Institute for Photonics and Advanced Sensing and the ARC Center for Nanoscale BioPhotonics, The University of Adelaide, Adelaide, SA, 5005, Australia (e-mail: Yinlan.Ruan@ adelaide.edu.au).

S.A. Vahid, was with The University of Adelaide, Adelaide, SA, 5005, Australia. He is now with the University of South Australia, Mawson Lakes, 5095, SA, Australia (Shahraam.AfsharVahid@unisa.edu.au).

H. Ebendoff-Heidepriem, is with the Institute for Photonics and Advanced Sensing and the ARC Center for Nanoscale BioPhotonics, The University of Adelaide, Adelaide, SA, 5005, Australia (e-mail: Heike.Ebendoff@ adelaide.edu.au).

T.M. Monro was with The University of Adelaide, Adelaide, SA, 5005, Australia. She is now with the University of South Australia, Adelaide, 5005, SA, Australia (Tanya.Monro@unisa.edu.au).

cylindrical vector modes: azimuthally polarized (TE_{01} mode), mixed polarized (hybrid HE_{21} mode) and radially polarized (TM_{01} mode) CV modes, which are typical with doughnut shapes. However in these fibers, TE_{01}, $HE_{21}^{even/odd}$ and TM_{01} modes (referred as CV modes for simplicity in the rest of the paper) have very close or nearly identical propagation constants β ($\beta=2\pi\times n_{eff}/\lambda$), where n_{eff} is the effective refractive index of the mode. The effective refractive index difference Δn_{eff} between these modes is usually in the order of 10^{-5} or less for these fibers. As a result, these modes are very sensitive to perturbations and the energy from one mode readily couples to the other mode, resulting in modes degeneracy and the formation of linearly polarized (referred as LP-modes) Hermite-Gaussian-like beams [19] which has fields distribution in two lobes and cannot efficiently switch off the fluorescence emission of the fluorophore in STED application. Significant differences in the propagation constants of the CV modes in a fiber are essential [19, 20] for high stability doughnut-shape mode propagation. Fibers with high numerical aperture (NA) have larger Δn_{eff} for higher order modes [20], which suggests a large core-cladding index contrast will support the more stable propagation of higher order modes. Specialty optical fiber can be designed with multilayer cladding of high material index contrast [19] to maximize the difference between the effective index of different modes and hence support the stable propagation of discrete higher order modes. Effective refractive index differences as high as 1.8×10^{-4} between n_{eff} of TM_{01} mode and other modes has been reported in [19], which allows TM_{01} mode propagation over more than 20 m within this novel fiber. A nanobore photonic crystal fiber was reported to be capable of maintaining TE_{01} and TM_{01} doughnut modes azimuthal and radial polarization along the fiber [21] with a hollow air channel sitting centrally in the fiber core.

In this paper, we propose a suspended core fiber with six struts (Fig. 1 (a)) for stable CV mode propagation. The suspended core structure enables large refractive index contrast of glass/air and small core size, leading to strong mode confinement, while providing higher mechanical strength in comparison with an unsupported step-index nanowire. Using a relatively large number of struts enables better circular symmetry of the core for the modes it guides, however it poses limitations to the fiber fabrication. For fiber preforms made using drilling or stacking, large number of struts requires larger number of circular preform holes which limits the minimum core size that can be achieved in the fiber using reasonable degree of hole inflation. For preforms made using extrusion, larger number of struts decreases the mechanical stability of the extrusion die. Here, we selected six struts as the best compromise between circular symmetry and ease of fabrication of the suspended core fiber.

For this six-strut suspended core structure, we have quantitatively investigated the effect of refractive index of the fiber material, core dimension and wavelength on the effective refractive index difference between TE_{01}, HE_{21} and TM_{01} modes (first higher order modes group), their maximum intensities of the doughnut crest (all intensities referred in this work are normalised by the total power of the mode) and the size of central dark region. In this work, we consider fiber materials with refractive indices in the range of 1.45 (silica) to 2.0 (tellurite). The simulations in this work show that a six-strut suspended core fiber with appropriate refractive index and core size can have a large Δn_{eff} in the order of 10^{-3} to 10^{-2} which supports stable propagation of radially and azimuthally polarized modes and has the potential to enable a fiber-based STED nanoscopy with nano scale resolution. In addition to achieving high Δn_{eff}, the proposed suspended core fiber supports the propagation of a fundamental Gaussian mode in the core for fluorophore excitation together with the doughnut mode for stimulated emission depletion in STED imaging application with different wavelengths.

II. Simulation of CV Modes in Six Struts Suspended Core Fiber

In this work, finite element software (COMSOL 3.4) was used to investigate the effective index, field intensity and central dark spot diameter for CV modes in a six-strut suspended core fiber for selected wavelength, core diameter and material refractive index.

The proposed six-strut suspended core fiber, whose cross-sectional structure is shown in Fig. 1 (a) (a fabricated F2 glass suspended core fiber with 2.06 μm core), has a quasi-step-index structure and a large core-cladding refractive index contrast (the cladding is predominantly comprised of air with refractive index of 1.0). The fiber supports a doughnut shaped beam (TE_{01}, HE_{21} or TM_{01} mode) residing predominantly in the high refractive index region (core), as shown in Fig. 1 (b). For a six-strut tellurite glass suspended core fiber (material index of 2.0) with 620 nm core diameter (used for Fig.1 (b)), the normalised intensity (which is normalized to the integral of the total fields of the fiber cross section as in the equation: $|E|^2/\sqrt{\iint(\boldsymbol{E}\times\boldsymbol{H})\cdot\boldsymbol{z}dA}$, where E and H are electric and magnetic field in respectively, z is the unit component along fiber axis z and dA is unit area) of the TM_{01} mode is in the order of 10^{12} and the full width at half maximum (FWHM) of the central dark spot is 196 nm at 750 nm wavelength).

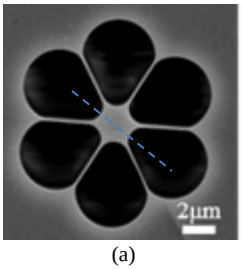

(a)

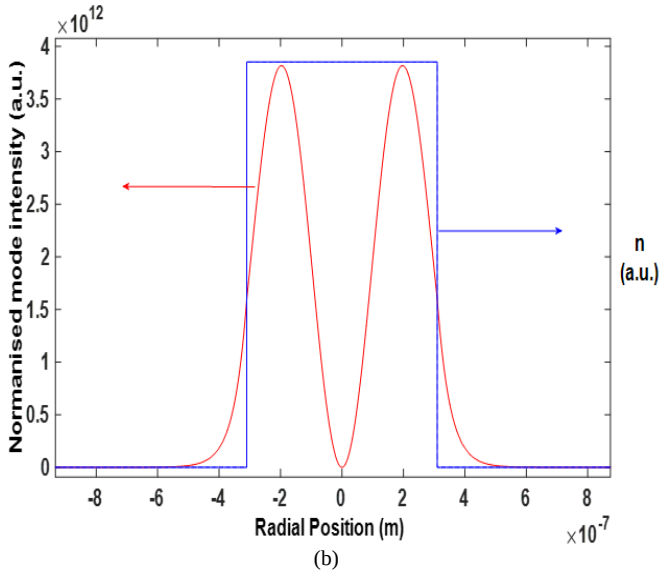

(b)

Fig. 1. (a) Schematic diagram of the cross-section of a suspended core fiber with six struts; (b) Schematic of TM_{01} mode field intensity and fiber refractive index profile at 750 nm wavelength for an ideal six struts suspended core fiber with 620 nm diameter and material index of 2.0 (tellurite glass) along a line crossing the core center as shown in schematic diagram (a).

We have investigated the field intensity and Δn_{eff} of CV modes in six-strut suspended core fibers at 750 nm wavelength with core diameters in the range of 550 nm to 5 µm and made from silica, F2 and tellurite glass having refractive indices of 1.454, 1.61 and 2.0, respectively. The CV modes field distribution, intensity (normalised) and effective index for each mode are calculated and evaluated. As an example, Fig. 2 shows the field intensity profiles for the first higher order CV modes, which include TE_{01}, $HE_{21}^{even/odd}$ and TM_{01} modes, in circular doughnut shape generated in six-strut suspended core fiber made of high-index tellurite glass and having a core diameter of 1.4 µm.

TM_{01} HE_{21}^{even}

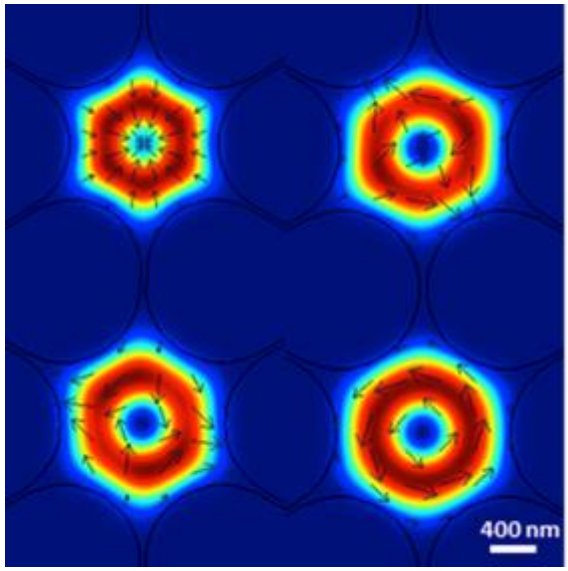

HE_{21}^{odd} TE_{01}

Fig. 2. Simulated CV modes intensity profile and field polarization distribution in a 1.4 µm diameter six-strut suspended core fiber made of high-index tellurite glass at 750 nm wavelength.

III. Results and Discussions

A. *Impact of Wavelength on Δn_{eff}*

We consider the impact of wavelength on effective index difference Δn_{eff} between TE_{01}, HE_{21} and TM_{01} in a 3 µm diameter core six-strut silica fiber in the wavelength range 200 nm – 1.5 µm. Fig. 3 shows that for 3 µm silica suspended core fiber, the absolute effective index difference, $|\Delta n_{eff}|$, steadily increases for both Δn_{eff} of TE_{01} (in red) and TM_{01} (in blue) relative to nearest neighboring HE_{21}. For shorter wavelengths of 450-800 nm, the Δn_{eff} is in the order of 10^{-4}, while for longer wavelengths up to 1.5 µm, the Δn_{eff} is up to the order of 10^{-3}. The reported highest Δn_{eff} achieved for the fibers are in order of 10^{-4} at 1500 nm and 1030 nm wavelengths, respectively [19, 20] (red spot [19] and black spot [20] in Fig. 3 for comparison).

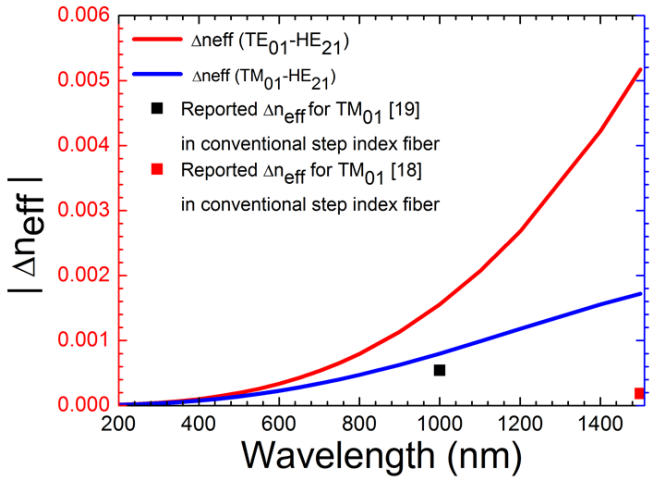

Fig. 3. Absolute effective index difference between TE_{01}, TM_{01} and HE_{21} CV modes as a function of wavelength for silica suspended core fiber with 3 µm core diameter in the wavelength range of 200-1500 nm.

The results in Fig. 3 show the six-strut suspended core fiber has a large Δn_{eff} between TE_{01} and HE_{21}, also TM_{01} and HE_{21} in a broad wavelength range, which is suitable for stable CV modes propagation. In the wavelength range of 200 – 1500 nm we studied, the Δn_{eff} between the fundamental Gaussian mode and the closest neighbor CV mode in a suspended core fiber is also increasing from order of 10^{-3} to 10^{-1} which suggest a stable Gaussian mode propagation. By reducing the core diameter of silica suspended core fiber to 0.55 – 1.1 µm, Δn_{eff} can be increased to the order of 10^{-2} at 750 nm wavelength, which is three order of magnitudes higher than that of conventional fibers [19]. As discussed in detail in the next section Δn_{eff} can be further increased by tuning the fiber material index.

B. Impact of Fiber Core Diameter and Material Index on Δn_{eff}

The effective index difference Δn_{eff} between the CV modes in a six-strut suspended core fiber was numerically examined for a range of fiber core diameters ranging from 550 nm to 4000 nm and for a variety of material refractive indices ranging from 1.454 (silica) to 2.0 (tellurite) at 750 nm wavelength.

First we consider Δn_{eff} between the azimuthally polarized TE_{01} mode and the nearest neighbor CV mode (TM_{01} or HE_{21}). The neighbor modes refer to the two modes with minimum index separation Δn_{eff}, and thus are most vulnerable to mode coupling. In some cases, TM_{01} mode has higher effective refractive index than the two degenerate HE_{21} modes, and vice versa for other core diameters. Fig.4 (a) shows that Δn_{eff} (in logarithmic scale) increases with decreasing core diameter. High Δn_{eff} of TE_{01} is observed for high index materials and small cores. For example, the high index tellurite fiber with 550 nm core diameter has a large Δn_{eff} of 0.0465 (-1.33 in log-scale). When moving to lower material indices (< 1.8), the maximum Δn_{eff} at a given material index corresponds to larger core diameters in the range of 550-900 nm. For example, the maximum Δn_{eff} of 0.0363, 0.0306, 0.0254 and 0.0161 (-1.44, -1.514, -1.595, -1.793 in log-scale) of fibers with material index n = 1.8, 1.7, 1.61 and 1.454 are found for core diameters of 650 nm, 700 nm, 750 nm and 900 nm, respectively. For the calculated materials, the minimum Δn_{eff} is greater than 1.7×10^{-4} (-3.8 in log-scale) which is for material index 2.0 and core diameter of 4000 nm except material with refractive index of 1.61. A minimum Δn_{eff} was observed for 1.61 material index and 550 nm core diameters fiber, in which the TE_{01} and TM_{01} modes become essentially degenerate with Δn_{eff} of 1×10^{-5} (-5.26 in log-scale), as shown in Fig. 4 (a).

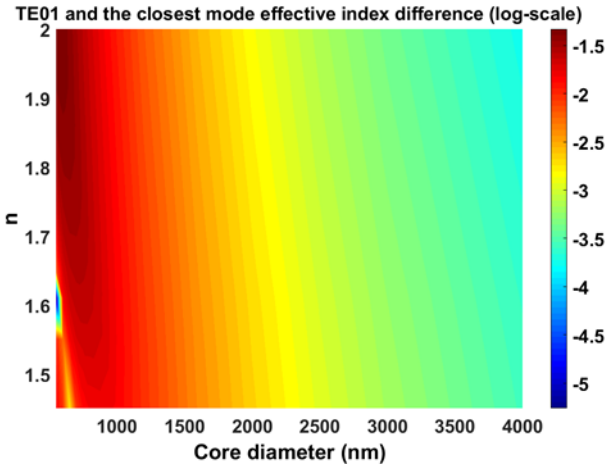

(a)

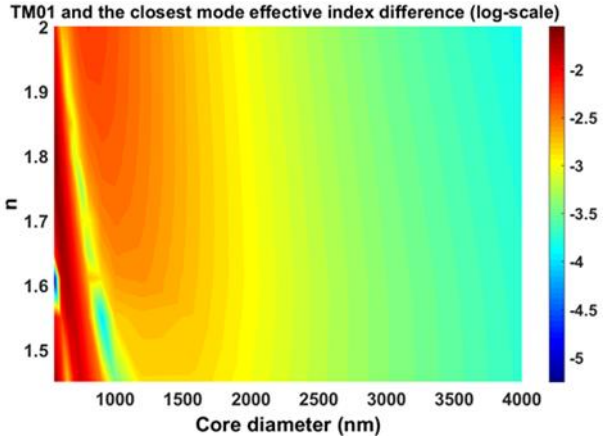

(b)

Fig. 4. Simulation results of the effective refractive index difference in logarithmic scale (negative value shown for color bar) between (a) the TE_{01} mode and the nearest neighbor mode, and (b) the TM_{01} and the nearest neighbor mode for different fiber core diameters and material refractive indices at wavelength of 750 nm.

Next we consider the impact of core diameter and material index on Δn_{eff} between the radially polarized TM_{01} mode and its nearest neighbor mode (Fig. 4(b)). Within the investigated core diameter range of 550 - 4000 nm, the maximum Δn_{eff} of TM_{01} is found for a smaller core compared to the Δn_{eff} for the TE_{01} mode. As the core diameter increases, Δn_{eff} of TM_{01} first decreases and then reaches a minimums at core diameters ranging from 600 nm for material index 2.0 to ~1000 nm for material index 1.45, as shown by the narrow strip of yellow to green color in Fig.4 (b). Within this strip, for 1.55 material index and 900 nm core diameter, the TM_{01} and the nearest neighbor mode become degenerate and have Δn_{eff} of 9.9×10^{-5} (-4.00 in log-scale). The maximum Δn_{eff} of 0.0239, 0.0149, 0.0182, 0.02 and 0.022 was found for material indices of 1.45, 1.55, 1.61, 1.65 and 1.7 and core diameters of 550, 650, 600 nm respectively (Fig. 4(b)). The minimum Δn_{eff} values are mostly larger than 1.44×10^{-4} (-3.84 in log-scale) except that of material index of 1.61 and core diameter of 550 nm, for which a Δn_{eff} in the order of 10^{-6} (-5.26 in log-scale) was observed.

Our calculation results show the azimuthally polarized TE_{01} and radially polarized TM_{01} modes have large Δn_{eff} to the nearest neighbor modes in a suspended core fiber with small core size. For most of materials and core diameters < 2 μm, both Δn_{eff} between TE_{01} and its neighbor, and that between TM_{01} and its neighbor are in the order of 10^{-2}~10^{-3}, except those singularities and degenerated strip as discussed above. For smaller cores (< 1 μm), higher material index leads to larger Δn_{eff}, while for larger cores (> 2.5 μm), Δn_{eff} for TE_{01} and TM_{01} modes show no significant change with increasing material index. For any mode of interest, the optimum material index and fiber core diameter combination can be identified from Fig. 4.

In order to gain a more detailed insight into the impact of material index and core diameter, the simulation results for low index silica fiber (n = 1.454) and high-index tellurite fiber (n = 2.0) at 750 nm wavelength and 500-2000 nm core diameters are plotted in Figs. 5 (a) and5 (b), respectively. The

aim of this analysis is to determine whether there is an advantage to use a high index fiber for STED nanoscopy. Due to the imaging optics used in the STED imaging setup, the radially polarized TM_{01} mode has a axial direction electric field component after it is focused onto a sample, which has an adverse effect to STED image resolution (but can be used for other applications, e.g. for electron acceleration [22]). By contrast, the azimuthally polarised TE_{01} mode in the fiber does not have the axial direction electric field component after being focused and therefore is more suitable for STED imaging application. Hence, we have mainly examined TE_{01} modes related properties for STED application, whereas we have only determined the effective indices for the HE_{21} and TM_{01} modes in order to calculate Δn_{eff} of TE_{01} and TM_{01} modes relative to their nearest neighbour modes. For both silica and tellurite fiber, the maximum field intensity of the TE_{01} mode increases and the diameter of the central dark spot decreases with decreasing core diameter (Fig. 5 (a)). For silica, the maximum intensity is obtained at a relatively small core diameter of 620 nm, while for high index tellurite no maximum is obtained even for the smallest core diameter investigated (550 nm). For core diameters in the range of 550-1200 nm, the TE_{01} mode intensity is in the order of 10^{12}. When the core diameter decreases to less than 620 nm, laser coupling efficiency, transmission and core mode confinement decrease [21,23], leading to a decline of the TE_{01} mode field intensity. As the resolution of STED is proportional to the doughnut beam intensity [24], the decrease in mode field intensity for the fibers with their core diameter < 620 nm core diameters results in STED resolution decrease.

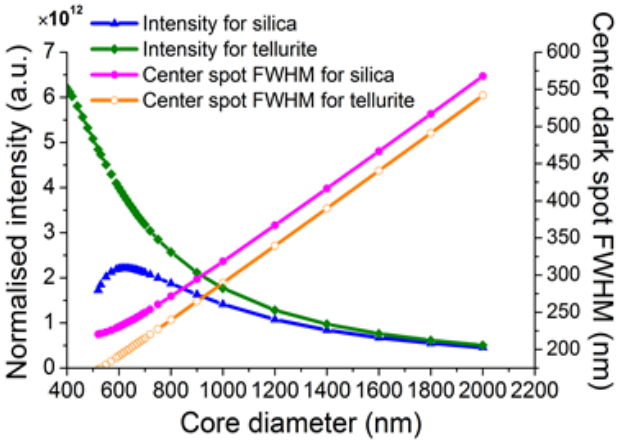

(a)

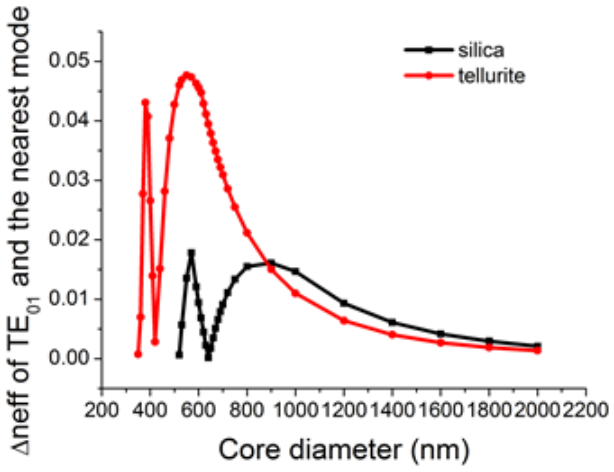

(b)

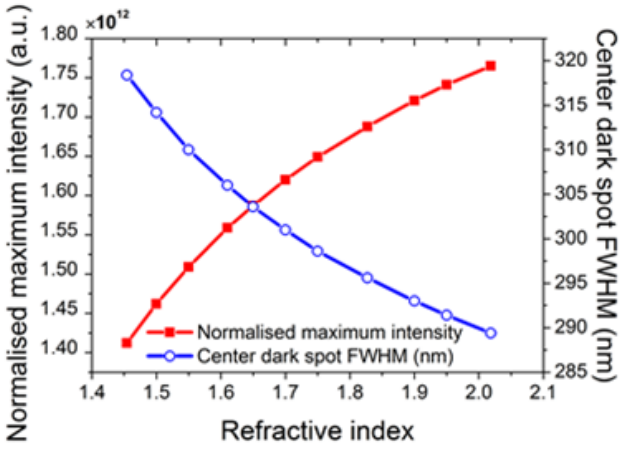

(c)

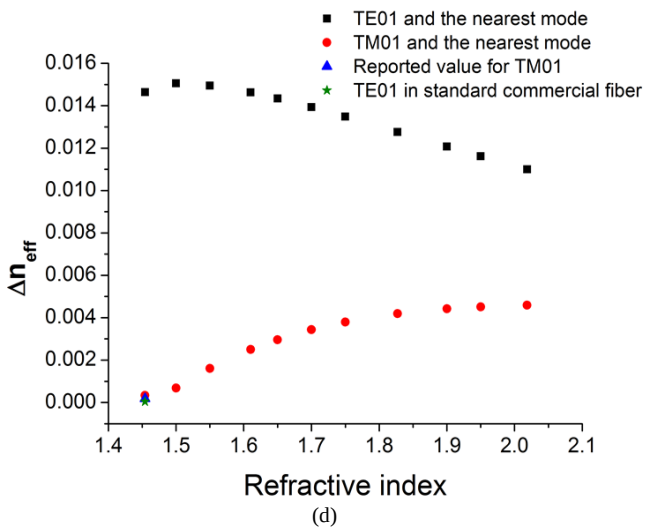

(d)

Fig. 5. Simulation results of (a) the TE_{01} mode field intensity and central dark spot size with varying core diameters for silica and tellurite fiber, (b) impact of core diameter on TE_{01} mode central dark spot size for silica and tellurite fiber, (c) impact of material refractive index on TE_{01} mode field intensity and the central dark spot size for core diameter of 1 μm and (d) effective refractive index difference between TE_{01} and HE_{21}, and between TM_{01} and HE_{21} modes for a 1 μm core diameter and 750 nm wavelength as a function of material refractive index.

For core diameters < 800 nm, the maximum intensity of the doughnut crest of high-index tellurite fiber is much higher than that of the low index silica fiber with the same core diameter. This suggests high refractive index fiber with small core size ranging from 550 nm to 1.5 μm can support a doughnut mode with higher maximum intensity compared to a low index fiber for the same excitation power. For core diameters > 1.5 μm, high-index and low-index fiber have comparable intensity scale.

As shown in Fig. 5 (b), as the core diameter decreases from 2 μm, Δn_{eff} between the TE_{01} mode and the nearest neighbor mode increases until ~900 nm core diameter for the silica fiber and ~500 nm core diameter for tellurite fiber. Further decrease of the core diameter results in a decrease of Δn_{eff}. Minimum Δn_{eff} is reached at core diameter of 670 nm for silica fiber and 440 nm for tellurite fiber which suggests with these dimensions and at the wavelength of 750 nm, the modes are crossing each other i.e., they are degenerate. Note that modes TE_{01} and HE_{21} are cut off when the core diameter is smaller than 510 nm for silica fiber and smaller than 350 nm for high index tellurite fiber. For core diameter > 950 nm, tellurite fiber has smaller Δn_{eff} between TE_{01} and the nearest neighboring mode. Most of the Δn_{eff} values are in the order of 10^{-3} - 10^{-2}. The modes that have small Δn_{eff} values in the order of 10^{-5}-10^{-6} are degenerated from practical application perspective. For core diameters >2 μm, both low index and high-index materials have Δn_{eff} values in the same order of magnitude.

The impact of the material index on intensity of the CV modes, central dark spot size as well as Δn_{eff} between higher order modes is shown in Figs. 5 (c) and (d). At a given core diameter, higher material index results in a doughnut beam with higher field intensity and smaller central dark spot. In Fig. 5 (d), the values of Δn_{eff} between TE_{01} or TM_{01} and the nearest neighbor mode (could be $HE_{21}^{even/odd}$ or, TM_{01} or TE_{01}) show different trends as the material index increases. The high Δn_{eff} of TE_{01} for low-index (~1.5) materials indicates higher mode propagation stability for TE_{01} in low-index fiber. By contrast, the high Δn_{eff} of the TM_{01} for high-index materials indicates higher mode propagation stability for TM_{01} in high-index material fiber.

The simulation results demonstrate that the suspended core fiber structure has the advantage that it allows larger Δn_{eff} between TE_{01} and HE_{21}, and between TM_{01} and HE_{21} to be achieved compared with conventional step-index fibers. For the suspended core fiber structure, the maximum Δn_{eff} between TE_{01} and HE_{21} is 1.5×10^{-2}, which is two orders of magnitude higher than that reported in [19] for a specially designed multilayer cladding step-index fiber (Δn_{eff} ~1.8×10^{-4}) and three orders of magnitude higher than that of conventional step-index fiber (Δn_{eff} ~10^{-5}). The high Δn_{eff} that can be achieved for the suspended core fiber structure demonstrates that this fiber structure supports more stable CV modes propagation.

For STED nanoscopy applications, the spatial resolution is a function of the spatial distribution and magnitude of the intensity of the doughnut shape depletion light [24]. The resolution can be estimated from the maximum intensity of the doughnut shape STED beam in a fiber at a given material index and core diameter based on equation (1). For example, when the maximum intensity of the doughnut STED beam crest for azimuthal TE_{01} mode in a fiber with diameter of 600 nm and 4W input power is about $I_m = 12\times10^{12}$ W/m^2, the STED beam wavelength is λ = 750 nm, the saturation intensity of the dye Atto-647N is I_S = 15 MW/cm^2, and an objective lens used to focus beams on sample with objective NA = 1.25, the spatial resolution is estimated to be 30 nm. For shorter STED beam wavelength of e.g. λ = 514 nm, NA = 1.4, $I_m = 12\times10^{12}$ W/m^2 (can be larger with higher input power) and lower I_S of ~ 2.9 MW/cm^2 (for dye Rhodamine B [25]) allows a spatial resolution of several nanometers to be achieved.

C. The Doughnut Beam Uniformity

In a suspended core fiber, struts are required to support the core. These struts have intersections with the core edge, which affects the doughnut beam distribution by virtue of the fact that the core is not circular in these regions. A doughnut beam with poor uniformity, which is defined as $(1-(I_{max}-I_{min})/(I_{max}+I_{min}))$ [15] (where I_{max} and I_{min} are normalised maximum intensity and minimum intensity respectively), has an adverse impact on the depletion region and hence on STED imaging efficiency. As both material index and core diameter can be used to tune Δn_{eff}, we examined the impact of these intersections on the TE_{01} mode doughnut beam uniformity for different fiber materials and core sizes. Fig. 6 (a) shows that the uniformity for material indices investigated (1.45 to 2.0) is larger than 99%, whereby the uniformity decreases towards higher material indices. Thus, varying material index has little effect on the doughnut field uniformity. Considering decreasing core diameter for silica fiber (Fig. 6 (b)), the doughnut beam uniformity first slightly increases from 2 μm to ~ 900 nm core diameter and then rapidly decreases for core diameters < 900 nm. For the material indices investigated, the TE_{01} doughnut beam uniformity is well above 99.5% for core diameters > 750 nm. In [15], maximum intensity uniformity around 87% has been achieved in a double-clad fiber, based on which and other experimental parameters the possibility of sub 100 nm resolution was predicted. The study here shows that high intensity uniformity > 95% can be potentially achieved for a wide range of parameters (refractive indices and core diameters) in six-strut fibers.

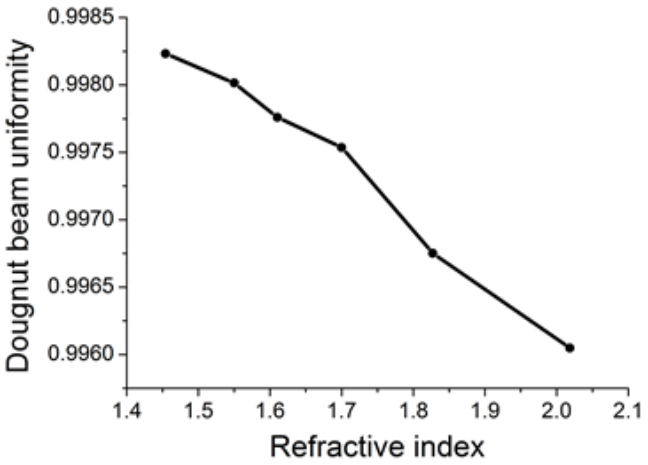

(a)

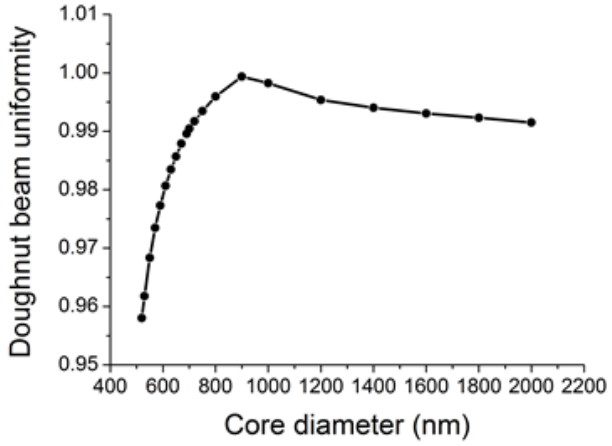

(b)

Fig. 6(a) Azimuthally polarised doughnut beam uniformity for 1 μm core diameter and 750 nm wavelength as a function of material refractive index; (b) doughnut beam uniformity for silica fiber at 750 nm wavelength as a function of core diameter.

Fiber core circularity is another critical factor which effects the doughnut beam uniformity. The simulation of the TE_{01} mode of a silica step index fiber with elliptical core (Fig. 7) demonstrates the field uniformity of this mode decreases with increasing core ellipticity. Since TE_{01} mode uniformity of 86.7% was shown to be sufficient to achieve high image resolution [15], ellipticity corresponding to uniformity larger than ~87% is considered to be acceptable. In a step index fiber with core ellipticity *e* of ~1.2% (ellipticity *e* = 1-b/a, where a of 860 nm and b of 850 nm are the major and minor radius of the fiber core, respectively) at 750 nm wavelength, the TE_{01} mode field has a uniformity of ~95.6%. The field profile of this mode is shown in Fig. 7 (b). For larger ellipticity of ~2.4%, the TE_{01} mode field uniformity has dropped to 91.3% (Fig. 7(c)), which is still above the acceptable value of ~87%. However, ellipticity of ~4.7% (Fig. 7 (d)) leads to a mode field uniformity below the acceptable level. The fabrication of a sub-micrometer suspended core fiber with ~ 2-3% ellipticity and thus acceptable uniformity is anticipated to be achievable with an improved fabrication process in the near future. The impact of ellipticity on the doughnut modes is under further investigation.

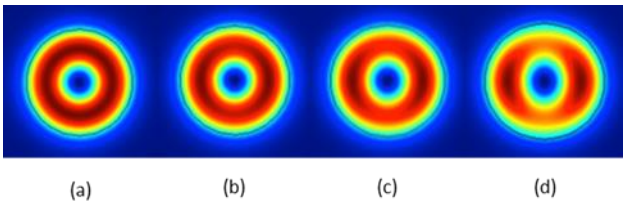

Fig. 7 Azimuthally polarised TE_{01} mode field profiles for (a) an ideal symmetric silica circular core of 0.85 μm diameter; (b) an elliptical core with ellipticity of ~1.1% and uniformity of 95.6%; (c) an elliptical core with ellipticity of ~2.4% and uniformity of 91.2% and (d) an elliptical core with ellipticity of ~4.7% and uniformity of 82.6% at 750 nm wavelength.

IV. Conclusions

In this work, we have shown that a six-strut suspended core fiber with appropriate material and small core diameter supports stable propagation of the TE_{01} mode (HE_{21} mode as well) and can be a competitive candidate to support stable propagation of CV modes. Our simulation results demonstrate that suspended core fibers have the advantage of large effective index differences between the first-higher order CV modes in order of 10^{-2}-10^{-3}, which lifts the high order modes' degeneracy and hence supports stable propagation of doughnut shaped beams by limiting the cross-talking between higher order modes. In a suspended core fiber, suitable selection of core diameter, operation wavelength and fiber material enables a uniform doughnut beam with high intensity and large Δn_{eff} between modes, which paves the way towards a fiber-based STED nanoscopy for imaging with high resolution of tens nanometers.

Acknowledgment

The authors acknowledge the support of the ARC Centre of Excellence for Nanoscale BioPhotonics. This work was performed in part at the OptoFab node of the Australian National Fabrication Facility (ANFF) utilizing Commonwealth and SA State Government funding.

References

[1] D. Wildanger, B.R. Patton, H. Schill, L. Marseglia, J.P. Hadden, S. Knauer, A. Schönle, J.G. Rarity, J.L. O'Brien, S.W. Hell, and J.M. Smith. (2012). Solid Immersion Facilitates Fluorescence Microscopy with Nanometer Resolution and Sub-Ångström Emitter Localization. *Adv. Mater. 24(44)*. pp. OP309-OP313.

[2] S.W. Hell and J. Wichmann. (1994). Breaking the diffraction resolution limit by stimulated emission: stimulated-emission-depletion fluorescence microscopy. *Opt. Lett. 19(11)*. pp. 780-782.

[3] T. Müller, C. Schumann, and A. Kraegeloh. (2012). STED microscopy and its applications: new insights into cellular processes on the nanoscale. *Chemphyschem. 13(8)*. pp. 1986-2000.

[4] B. Harke, S.W. Hell, R. Medda, and K.I. Willig. (2007, Nov.) STED microscopy with continuous wave beams. *Nat. Methods. 4(11)*. pp. 915+.

[5] C. Eggeling, K.I. Willig, and F.J. Barrantes. (2013,) STED microscopy of living cells – new frontiers in membrane and neurobiology. *J. Neurochem. 126(2)*. pp. 203-212.

[6] C. Varin and M. Piché. (2002). Acceleration of ultra-relativistic electrons using high-intensity TM01 laser beams. *Appl. Phys. B. 74(1)*. pp. s83-s88.

[7] Q. Zhan. (2004). Trapping metallic Rayleigh particles with radial polarization. *Opt. Express. 12(15)*. pp. 3377-3382.
[8] L. Novotny, M.R. Beversluis, K.S. Youngworth, and T.G. Brown. Longitudinal Field Modes Probed by Single Molecules.(2001). *Phy. Rev. Lett. 86(23)*. pp. 5251-5254.
[9] A.V. Nesterov and V.G. Niziev. (2000). Laser beams with axially symmetric polarization. *J. Phys. D-Appl. Phys. 33(15)*. pp. 1817-1822.
[10] A. Vaziri, G. Weihs, and A. Zeilinger. (2002). Experimental two-photon, three-dimensional entanglement for quantum communication. *Phys. Rev. Lett. 89(24)*. pp. 240401.
[11] G. Gibson, J. Courtial, M.J. Padgett, M. Vasnetsov, V. Pas'ko, S.M. Barnett, and S. Franke-Arnold. (2004). Free-space information transfer using light beams carrying orbital angular momentum. *Opt. Express. 12(22)*. pp. 5448-5456.
[12] C. Gabriel, A. Aiello, W. Zhong, T.G. Euser, N.Y. Joly, P. Banzer, M. Förtsch, D. Elser, U.L. Andersen, Ch. Marquardt, P.St. J. Russell, and G. Leuchs. (2011). Entangling different degrees of freedom by quadrature squeezing cylindrically polarized modes. *Phys. Rev. Lett. 106(6)*. pp. 060502.
[13] L. Gruner-Nielsen, Y. Sun, J.W. Nicholson, D. Jakobsen, K.G. Jespersen, R. Lingle, and B. Palsdottir. (2012). Few mode transmission fiber with low DGD, low mode coupling, and low loss. *J. Lightw. Technol. 30(23)*. pp. 3693-3698.
[14] N. Bozinovic, Y. Yue, Y. Ren, M. Tur, P. Kristensen, H. Huang, A.E. Willner, and S. Ramachandran. (2013, Jul.). Terabit-scale orbital angular momentum mode division multiplexing in fibers. *Science. 340(6140)*. pp. 1545-1548.
[15] M. Gu, H. Kang, and X. Li. (2014, Jan.). Breaking the diffraction-limited resolution barrier in fiber-optical two-photon fluorescence endoscopy by an azimuthally-polarized beam. *Sci. Rep. 4*. pp. 3627.
[16] J. Demas, M.D.W. Grogan, T. Alkeskjold, and S. Ramachandran. (2012, Sep.). Sensing with optical vortices in photonic-crystal fibers. *Opt. Lett. 37(18)*. pp. 3768-3770.
[17] L. Yan, E. Auksorius, N. Bozinovic, G.J. Tearney, and S. Ramachandran. (2013, Jun.). *Optical Fiber Vortices for STED Nanoscopy*. Presented at *CLEO: 2013*. [online]. Available: https://www.osapublishing.org/abstract.cfm?uri=CLEO_SI-2013-CTu3N.2
[18] J.-i. Hotta, E. Fron, P. Dedecker, K.P.F. Janssen, C. Li, K. Müllen, B. Harke, J. Bückers, S.W. Hell, and J. Hofkens. (2010). Spectroscopic rationale for efficient stimulated-emission depletion microscopy fluorophores. *J. Am. Chem. Soc. 132(14)*. pp. 5021-5023.
[19] S. Ramachandran, P. Kristensen, and M.F. Yan. (2009). Generation and propagation of radially polarized beams in optical fibers. *Opt. Lett. 34(16)*. pp. 2525-2527.
[20] C. Jocher, C. Jauregui, C. Voigtlander, F. Stutzki, S. Nolte, J. Limpert, and A. Tunnermann. (2011). Fiber based polarization filter for radially and azimuthally polarized light. *Opt. Express. 19(20)*. pp. 19582-19590.
[21] T.G. Euser, M.A. Schmidt, N.Y. Joly, C. Gabriel, C. Marquardt, L.Y. Zang, M. Fortsch, P. Banzer, A. Brenn, D. Elser, M. Scharrer, G. Leuchs, and P.S. Russell. (2011). Birefringence and dispersion of cylindrically polarized modes in nanobore photonic crystal fiber. *J. Opt. Soc. Am. B-Opt. Phys. 28(1)*. pp. 193-198.
[22] Y.I. Salamin. (2006). Electron acceleration from rest in vacuum by an axicon Gaussian laser beam. *Phy. Rev. A. 73(4)*. pp. 043402(6).
[23] H. Ebendorff-Heidepriem, S.C. Warren-Smith, and T.M. Monro. (2009). Suspended nanowires: fabrication, design and characterization of fibers with nanoscale cores. *Opt. Express. 17(4)*. pp. 2646-2657.
[24] B. Harke, J. Keller, C.K. Ullal, V. Westphal, A. Schönle, and S.W. Hell. (2008). Resolution scaling in STED microscopy. *Opt. Express. 16(6)*. pp. 4154-4162.
[25] D.R. Sandison, R. M. Williams, K. S. Wells, J. Strickler, and W.W. Webb, "Quantitative fluorescence confocal Laser Scanning microscopy(CLSM)" in *Handbook of Biological Confocal Microscopy*, 2nd. ed., J. Pawley, Ed. Boston MA: Springer US, 1995, pp. 39-53.

Hong Ji received the B.Sc. degree in applied physics from Fuzhou University, Fuzhou, China and Master degree in the University of Wollongong. Her research interests include optical fiber material, optical fiber sensor, and fiber imaging device, fiber gratings and photonic crystal technology.

Yinlan Ruan gained her PhD from the Australian National University, Australia in 2006 with her thesis title of chalcogenide planar waveguide devices for all-optical processing. She joined School of Physical Science, University of Adelaide in 2006. Since then, Dr Ruan has worked in the diversified projects including fluoride glass development, biosensing, subwavelength fibres, graphene integration with optical fibers and nanodiamond-tellurite hybrid fibers. Her current interests is high resolution imaging, optical biochemical sensing and generation of single photon sources.

Shahraam Afshar Vahid received the Ph.D. degree in physics, laser and nonlinear optics from the University of Adelaide. From 1998 to 2001 he held a Lecturer A position at The University of Adelaide. In 2001 he joined the fiber optics group at The University of Ottawa as a postdoc, where he worked on fiber-optic, distributed strain and temperature sensors based on Brillouin scattering. In 2003, he received the NCIT Fellowship from the National Capital Institute of Telecommunication, Canada, to work on Brillouin scattering in photonic crystal fibers. In 2005, he joined Prof. Tanya Monro to establish The Centre of Expertise in Photonics (CoEP) at the University of Adelaide. Since then, he has had significant roles in establishing the research directions of CoEP, setting up the CoEP labs, supervising honours and Ph.D. students and initiating and developing different projects. His current research within the Centre of Expertise in Photonics focuses on nonlinear optical phenomena in microstructured fibers, bandgap fibers, chem/biosensing using optical fibers, and TeraHerz waveguides. Since 2009, he has been appointed as a Lecturer at The University of Adelaide. He currently hold an A/professor at University of South Australia.

Heike Ebendorff-Heidepriem received the Ph.D. degree in chemistry from the University of Jena, Germany, in 1994, where she continued her research on optical glasses until 2000. During 2001-2004 she was with the Optoelectronics Research Centre at the University of Southampton, UK, working on novel photosensitive glasses and soft glass microstructured optical fibers with record high nonlinearity. Since 2005, she has been with the University of Adelaide, Australia. Currently, she is one of the leaders of the Optical Materials & Structures Science Theme and the Deputy Director of the Institute for Photonics and Advanced Sensing. She was awarded the Woldemar A. Weyl International Glass Science Award and a prestigious EU

Marie Curie Individual Fellowship in 2001. Her research focuses on the development of novel optical glasses, fibers, surface functionalization and sensing approaches.

Tanya M. Monro received the Ph.D. degree in physics from the University of Sydney, NSW, Australia, in 1998, for which she was awarded the Bragg Gold Medal for the best Physics Ph.D. in Australia.

In 2000, she received a Royal Society University Research Fellowship at the Optoelectronics Research Centre at the University of Southampton, U.K. She came to the University of Adelaide in 2005 as an inaugural Chair of Photonics. She was the inaugural Director of the Institute for Photonics and Advanced Sensing from 2008 to August 2014 and of the ARC Centre of Excellence for Nanoscale BioPhotonics, University of Adelaide. She is currently an Australian Research Council Georgina Sweet Laureate Fellow and the Deputy Vice Chancellor Research and Innovation at the University of South Australia. Her research interests include nanophotonics, optical fiber biosensing and novel laser architectures.

Dr. Monro received the Australia Academy of Sciences Pawsey Medal for 2012 and in 2011, South Australia's "Australian of the Year," and the Scopus Young Researcher of the Year. In 2010, she was named South Australian Scientist of the Year and Telstra Business Women of the Year (in the Community &Government category). In 2008, she received the Prime Minister's Malcolm McIntosh Prize for Physical Scientist of the Year. She is a Fellow of the Australian Institute of Physics. She is a Member of the South Australian Economic Development Board and the Commonwealth Science Council.